

A Model for Colour Prediction of Halftoned Samples Incorporating Light Scattering and Ink Spreading*

*Patrick Emmel, Roger David Hersch
Ecole Polytechnique Fédérale de Lausanne (EPFL),
CH-1015 Lausanne, Switzerland.
Patrick.Emmel@epfl.ch, Rd.Hersch@epfl.ch*

Abstract

This study introduces new models and mathematical formulations describing the light scattering and ink spreading phenomena. Based on these new theoretical tools, the spectra of 100 real paper samples produced by two ink-jet printers were computed with an average prediction error of about $\Delta E = 2.1$ in CIELAB.

Keywords: spectral colour prediction, light scattering, ink spreading, halftones, ink-jet printing.

Introduction

Several physical phenomena influence colours reproduced by ink-jet printers. This makes accurate colour prediction very difficult. The dot gain effect is generally considered to have the largest impact on colour deviations. Dot gain is caused by light scattering or by ink spreading or both together.

Intensive investigations on optical dot gain (Yule-Nielsen effect) have been made,^{2,10,25} but the resulting prediction models are often very complex. We propose a global approach incorporating all physical contributing phenomena into a single model using a mathematical framework based on matrices. We will show that classical results (for example the Clapper-Yule relation) correspond to particular cases of our model.

According to our experience in ink-jet printing, light scattering is not the only process which induces colour deviations. When ink drops are printed over each other or just overlap partially, an ink spreading process takes place which also modifies the printed colour in a significant way. A model is proposed and applied to predict accurately the spectra of real samples produced with two inks on two different ink-jet printers.

Matrix form of the Kubelka-Munk model

Let us consider a reflector made of a reflecting substrate of reflectance R_g in optical contact with a light absorbing and light scattering medium of thickness X (see Figure 1). Kubelka and Munk¹⁶ proposed a reflection model based on two light fluxes: $i(x)$ oriented downwards and $j(x)$ oriented upwards.

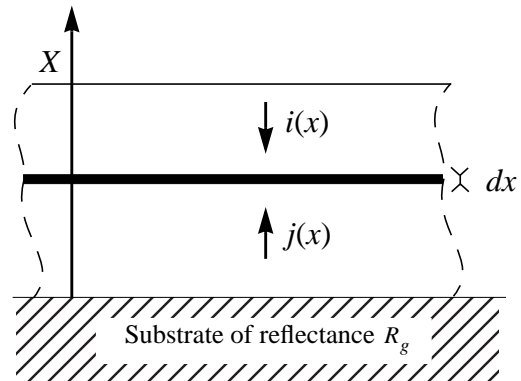


Figure 1. An ink absorbing medium of thickness X is in optical contact with a substrate of reflectance R_g . This medium is divided into parallel layers of infinitesimal thickness dx . Two fluxes are considered: $i(x)$ oriented downwards and $j(x)$ oriented upwards.

The variation of $i(x)$ and $j(x)$ when they cross an infinitesimal layer of thickness dx is given by the system of linear differential equations:

$$\begin{cases} \frac{di(x)}{dx} = (K + S)i(x) - S j(x) \\ \frac{dj(x)}{dx} = -(K + S)j(x) + S i(x) \end{cases} \quad (1)$$

where K is the light absorption coefficient and S the light scattering coefficient of the medium. Note that in a transparent medium S equals 0 and the differential equation (1) leads to Beer's law.

The system in equation (1) can be written in matrix form:

$$\begin{bmatrix} \frac{di(x)}{dx} \\ \frac{dj(x)}{dx} \end{bmatrix} = \begin{bmatrix} K + S & -S \\ S & -(K + S) \end{bmatrix} \cdot \begin{bmatrix} i(x) \\ j(x) \end{bmatrix} \quad (2)$$

This kind of matrix differential equation has a well known solution which is given by the exponential of the matrix.⁴ By integrating the equation between $x = 0$ and $x = X$ we get:

* Proceedings of the IS&T/SID 7th Color Imaging Conference: Color Science, Systems and Applications, November 16-19, 1999, Scottsdale, Arizona, USA, pp. 173-181.

$$\begin{bmatrix} i(X) \\ j(X) \end{bmatrix} = \exp\left(\begin{bmatrix} K+S & -S \\ S & -(K+S) \end{bmatrix} (X-0)\right) \cdot \begin{bmatrix} i(0) \\ j(0) \end{bmatrix} \quad (3)$$

where $i(0)$ and $j(0)$ are the intensities of the fluxes i and j at $x = 0$. Note that the exponential of a matrix M is defined by the following power series:

$$\exp(M) = \sum_{i=0}^{\infty} \frac{(M)^i}{i!} \quad (4)$$

The ratio $\rho = j(X)/i(X)$ is called the body (or true) reflectance¹⁹ of the analysed sample. It corresponds to an internal reflection coefficient which does not take multiple internal reflections into account (see following section). From equation (3) and the boundary condition $j(0) = R_g \cdot i(0)$, we can derive by algebraic manipulations all the well-known results of the Kubelka-Munk theory which are listed in the literature.^{6,8,14}

Model of high quality paper and Saunderson correction

In the present study, we consider high quality ink-jet paper consisting of an ink-absorbing layer in optical contact with the substrate which is a diffuse white reflector of reflectance R_g . This reflector is supposed to be Lambertian¹⁷ and is never in contact with the inks. Since the transparent coating has a refractive index n different from that of air, multiple internal reflections occur¹³ as shown in Figure 2. This phenomenon significantly increases the optical density of the ink containing layer. Traditionally, this is taken into account by applying the Saunderson correction¹⁸ to the computed spectrum. In this section, we write the Saunderson correction in matrix form, to be applied to equation (3).

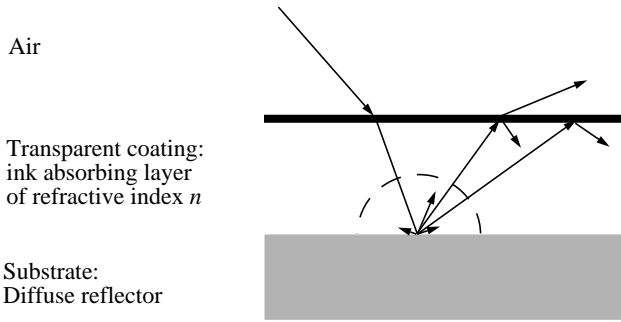


Figure 2. Multiple internal reflections caused by the interface between the air and the ink-coating.

Let us denote by i the incident flux on the external surface of the paper and by j the flux emerging from the paper. Let r_s be the fraction of diffuse light reflected by the air-coating interface (external surface of the paper), and let r_i be the fraction of diffuse light reflected by the air-coating interface (internal surface of paper). The values of r_s and r_i depend only on the refractive index of the transparent coating. Judd¹² has computed their numerical values for a large number of refractive indices.

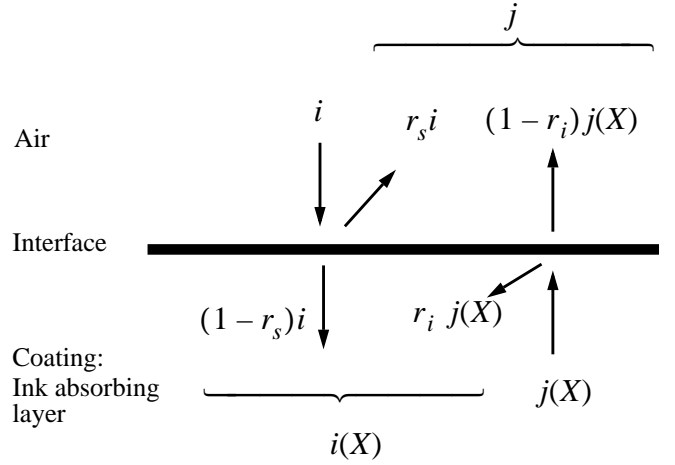


Figure 3. External and internal reflections of the upward and downward fluxes on the air-coating interface.

The balance of the fluxes at the air-coating interface, as shown in Figure 3, leads to the following system of equations for $i(X)$, the incident flux below the air-coating interface and for j , the emerging flux above the air-coating interface:

$$\begin{aligned} i(X) &= (1-r_s)i + r_i j(X) \\ j &= r_s i + (1-r_i)j(X) \end{aligned} \quad (5)$$

Assuming that the refractive index of the coating is constant over the whole visible range of wavelengths, r_s and r_i are also constant. Hence, equation (5) can be written in the following matrix form:

$$\begin{bmatrix} i \\ j \end{bmatrix} = \begin{bmatrix} \frac{1}{1-r_s} & \frac{-r_i}{1-r_s} \\ \frac{r_s}{1-r_s} & \left(1-r_i - \frac{r_s r_i}{1-r_s}\right) \end{bmatrix} \begin{bmatrix} i(X) \\ j(X) \end{bmatrix} \quad (6)$$

The Saunderson correction is obtained by combining equation (6) and equation (3):

$$\begin{aligned} \begin{bmatrix} i \\ j \end{bmatrix} &= \begin{bmatrix} \frac{1}{1-r_s} & \frac{-r_i}{1-r_s} \\ \frac{r_s}{1-r_s} & \left(1-r_i - \frac{r_s r_i}{1-r_s}\right) \end{bmatrix} \cdot \exp\left(\begin{bmatrix} K+S & -S \\ S & -(K+S) \end{bmatrix} X\right) \cdot \begin{bmatrix} i(0) \\ j(0) \end{bmatrix} \\ &= \begin{bmatrix} t & u \\ v & w \end{bmatrix} \cdot \begin{bmatrix} i(0) \\ j(0) \end{bmatrix} \end{aligned} \quad (7)$$

We denote the elements of the product matrix by t , u , v and w . These coefficients and the boundary condition $j(0) = R_g \cdot i(0)$ allow the calculation of the reflection coefficient R :

$$R = \frac{j}{i} = \frac{t + R_g \cdot u}{v + R_g \cdot w} \quad (8)$$

This equation allows us to compute the reflection spectrum of a light-absorbing and light-scattering medium in optical contact with a substrate of known reflectance R_g . If we develop the product in equation (8) algebraically, we obtain the famous Saunderson corrected reflection formula.²⁷ The interesting aspect of our present approach is the matrix formulation of equation (7) which gives a better overview of the modelled system. Instead of using several functions incorporated within each other, the analysed sample is simply modelled by the product of two matrices.

New mathematical framework for light scattering in the substrate

The Kubelka-Munk model presented in the previous sections assumes that the ink-absorbing layer is uniform, i.e. that it contains the same amount of dye everywhere. In halftoned prints, this is no longer true because ink was not applied uniformly over the whole surface. Due to light scattering in the substrate (paper), a photon can penetrate the paper through an inked region and leave the paper through a non-inked region.

In a first step, we generalise the previous model by taking only two types of regions into account: inked and non-inked. Furthermore, since the ink absorbing layer is very thin (about $10\mu m$), we assume that the exchange of photons between surface elements only takes place in the substrate. We also assume that each surface element behaves according to the Kubelka-Munk model described previously.

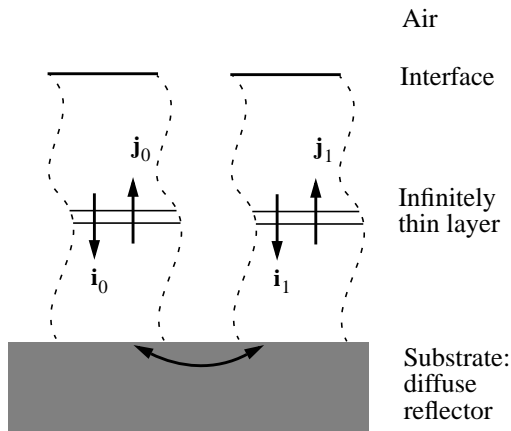


Figure 4. Model of the printed surface. On top of the substrate, each surface-element is considered to be a uniform layer which behaves according to the Kubelka-Munk model. The exchange of photons between different regions takes place in the substrate.

Let us now consider such a surface having only two different inking levels. As for the Kubelka-Munk model, we define for each inking level two light fluxes: i_k oriented downwards and j_k oriented upwards. The index k takes the value 0 for the non-inked region and 1 for the inked region (see Figure 4).

The matrix equation (2) can be extended in order to take several inking levels into account. For two inking levels, the equation can be written as follows:

$$\begin{bmatrix} \frac{di_0(x)}{dx} \\ \frac{di_1(x)}{dx} \\ \frac{dj_0(x)}{dx} \\ \frac{dj_1(x)}{dx} \end{bmatrix} = \begin{bmatrix} K_0 + S_0 & 0 & -S_0 & 0 \\ 0 & K_1 + S_1 & 0 & -S_1 \\ S_0 & 0 & -(K_0 + S_0) & 0 \\ 0 & S_1 & 0 & -(K_1 + S_1) \end{bmatrix} \cdot \begin{bmatrix} i_0(x) \\ i_1(x) \\ j_0(x) \\ j_1(x) \end{bmatrix} \quad (9)$$

where K_0 , S_0 , K_1 and S_1 are respectively the absorption and scattering coefficients of the non-inked medium and the inked medium. By integrating equation (9) between $x = 0$ and $x = X$ we get:

$$\begin{bmatrix} i_0(X) \\ i_1(X) \\ j_0(X) \\ j_1(X) \end{bmatrix} = \exp \left(\begin{bmatrix} K_0 + S_0 & 0 & -S_0 & 0 \\ 0 & K_1 + S_1 & 0 & -S_1 \\ S_0 & 0 & -(K_0 + S_0) & 0 \\ 0 & S_1 & 0 & -(K_1 + S_1) \end{bmatrix} \cdot X \right) \cdot \begin{bmatrix} i_0(0) \\ i_1(0) \\ j_0(0) \\ j_1(0) \end{bmatrix} \quad (10)$$

Note that the definition of the matrix exponential is given in equation (4).

In order to take into consideration the multiple internal reflections, the Saunderson correction must also be applied here. Note that in our case the ink is inside the medium and not on top of it. Hence the interface between the air and the ink absorbing medium is the same in non-inked regions and in inked regions. Therefore, from equation (6) we can directly derive the resulting correction matrix:

$$\begin{bmatrix} i_0 \\ i_1 \\ j_0 \\ j_1 \end{bmatrix} = \begin{bmatrix} \frac{1}{1-r_s} & 0 & \frac{-r_i}{1-r_s} & 0 \\ 0 & \frac{1}{1-r_s} & 0 & \frac{-r_i}{1-r_s} \\ \frac{r_s}{1-r_s} & 0 & \left(1-r_i - \frac{r_s r_i}{1-r_s}\right) & 0 \\ 0 & \frac{r_s}{1-r_s} & 0 & \left(1-r_i - \frac{r_s r_i}{1-r_s}\right) \end{bmatrix} \begin{bmatrix} i_0(X) \\ i_1(X) \\ j_0(X) \\ j_1(X) \end{bmatrix} \quad (11)$$

The key to our model lies in the way light scattering is expressed mathematically. We assume that the exchange of photons only takes place in the substrate. In consequence, the light scattering only affects the boundary conditions at $x = 0$. This implies that the upwards oriented fluxes $j_0(0)$ and $j_1(0)$ depend on both downwards oriented fluxes $i_0(0)$,

$i_1(0)$ and the reflection coefficient R_g of the substrate. This can be written in a general way under matrix form:

$$\begin{bmatrix} j_0(0) \\ j_1(0) \end{bmatrix} = R_g \cdot \begin{bmatrix} \delta_{0,0} & \delta_{0,1} \\ \delta_{1,0} & \delta_{1,1} \end{bmatrix} \cdot \begin{bmatrix} i_0(0) \\ i_1(0) \end{bmatrix} \quad (12)$$

where the coefficient $\delta_{u,v}$ represents the probability of a photon entering through a surface element having the inking level v to emerge from a surface element having the inking level

u . This probabilistic approach was introduced by Arney.^{1,2} Since we deal with probabilities, the sum of the coefficients $\delta_{u,v}$ belonging to the same line of the matrix in equation (12) must equal 1. The computation of the scattering probabilities $\delta_{u,v}$ will be addressed in the next section.

Now we can put all elements together and write the matrix equation of our new prediction model. By combining equations (10), (11) and (12) we obtain relation (13).

$$\begin{bmatrix} i_0 \\ i_1 \\ j_0 \\ j_1 \end{bmatrix} = \begin{bmatrix} \frac{1}{1-r_s} & 0 & \frac{-r_i}{1-r_s} & 0 \\ 0 & \frac{1}{1-r_s} & 0 & \frac{-r_i}{1-r_s} \\ \frac{r_s}{1-r_s} & 0 & \left(1-r_i-\frac{r_s r_i}{1-r_s}\right) & 0 \\ 0 & \frac{r_s}{1-r_s} & 0 & \left(1-r_i-\frac{r_s r_i}{1-r_s}\right) \end{bmatrix} \cdot \exp \left(\begin{bmatrix} K_0+S_0 & 0 & -S_0 & 0 \\ 0 & K_1+S_1 & 0 & -S_1 \\ S_0 & 0 & -(K_0+S_0) & 0 \\ 0 & S_1 & 0 & -(K_1+S_1) \end{bmatrix} \cdot X \right) \cdot \begin{bmatrix} 1 & 0 & 0 & 0 \\ 0 & 1 & 0 & 0 \\ 0 & 0 & \delta_{0,0} & \delta_{0,1} \\ 0 & 0 & \delta_{1,0} & \delta_{1,1} \end{bmatrix} \cdot \begin{bmatrix} i_0(0) \\ i_1(0) \\ R_g i_0(0) \\ R_g i_1(0) \end{bmatrix} \quad (13)$$

The first matrix of equation (13) represents the Saunderson correction, the second matrix corresponds to the Kubelka-Munk modelling of the ink absorbing layer and the third matrix models the light scattering in the substrate.

After computing the matrix products in equation (13), we can derive a relation which expresses the emerging fluxes j_0 and j_1 as linear functions of the incident fluxes i_0 and i_1 .

Since the incident light has the same intensity on inked and non-inked regions, we have $i_0 = i_1 = i$. Let a_1 be the fraction of area occupied by inked regions, and $a_0 = 1 - a_1$ be the fraction of area occupied by non-inked regions. The reflection coefficient R of the whole surface is given by:

$$R = \frac{\begin{bmatrix} a_0 & a_1 \end{bmatrix} \cdot \begin{bmatrix} j_0 \\ j_1 \end{bmatrix}}{\begin{bmatrix} a_0 & a_1 \end{bmatrix} \cdot \begin{bmatrix} i_0 \\ i_1 \end{bmatrix}} = \frac{(1-a_1)j_0 + a_1j_1}{i} \quad (14)$$

Let us consider the particular case in which the average lateral light scattering distance is great compared to the size of the halftone element. In this case, for any inking level v , the probability $\delta_{u,v}$ equals the fraction of area a_u occupied by the inking level u :

$$\delta_{0,0} = \delta_{1,0} = a_0 = 1 - a_1 \text{ and } \delta_{0,1} = \delta_{1,1} = a_1 \quad (15)$$

By introducing the relations (15) in equation (13) and assuming that $S_k = 0$, $K_0 = 0$, we obtain from expression (14) the well-known Clapper-Yule⁵ relation:

$$R = r_s + \frac{R_g(1-r_s)(1-r_i)(1-a_1+a_1T)^2}{1-R_g r_i(1-a_1+a_1T^2)} \quad (16)$$

where $T = \exp[-K_1X]$. Note that this calculation was done with the help of a mathematics software package.

In another particular case, lateral light scattering can be neglected. Hence, the probability of a photon being scattered in a region with a different inking level equals 0. This implies that $\delta_{u,u} = 1$ and $\delta_{u,v} = 0$ for $u \neq v$. In other words, the last matrix of equation (13) is an identity matrix. Introducing this in relation (13) and assuming $S_k = 0$, $K_0 = 0$, $r_i = 0$, $r_s = 0$ leads to the Murray-Davis relation:¹⁵

$$R = R_g[(1-a_1) + a_1T^2] \quad (17)$$

where $T = \exp[-K_1X]$.

Simplified light scattering model

There are several methods which allow the computation of the scattering probabilities $\delta_{u,v}$. Most of these methods use a point spread function (PSF) which is generally assumed or measured empirically. The convolution between this function and the halftone pattern leads to the surface reflectance²⁶ from which the scattering probabilities are deduced. Further advanced models calculate the PSF based on a physical light scattering model.²⁴ Since these methods imply the use of operations such as Fourier transforms, the computation is cumbersome. Finally, the scattering probabilities $\delta_{u,v}$ can also be computed by a numerical simulation based on a simplified light scattering model.¹⁰

For our purpose, the last method is the most adapted: a high resolution grid models the printed surface. The value of a grid point corresponds to the local amount of dye (see Figure 5). The density profile of an isolated ink impact was measured under a microscope and approximated by a parabolic function.⁷ The resulting ink impact model (see Figure 5)

is used as a stamp. Wherever an ink drop hits the surface of the printed media, the impact model is stamped at the same location on the high resolution grid, where stamp overlapping is additive. This gives an accurate numerical simulation of the behaviour of ink printed on high quality paper.

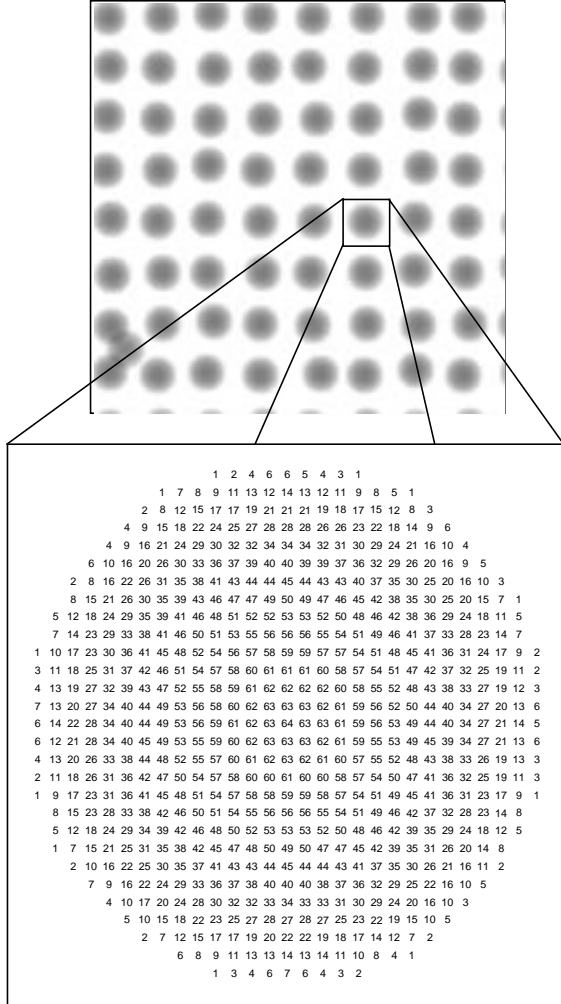


Figure 5. High resolution grid modelling the printed surface. The value of a grid point corresponds to the local amount of dye. Note that the density profile of an isolated ink impact is parabolic.

The fraction of area a_u is determined by counting the number of grid points which belong to the same inking level u . The light scattering process can be seen as an exchange of photons between a grid point and its neighbours. In this context, the discrete form of the above mentioned PSF gives the probability for an entering photon to emerge from another grid point. According to Gustavson's studies,¹¹ this PSF can be approximated by a function $p(r)$ which has a circular symmetry and a strong radial decay:

$$p(r) = \frac{\exp\left[-\frac{r}{d}\right]}{2\pi dr} \quad (18)$$

Here, d controls the radial extent of the PSF.

The scattering probability $\delta_{u,v}$ equals the weighted sum over the whole grid of points having the inking level u with a neighbour having an inking level v . The weights of the neighbours are given by our discrete PSF.

A simplified model of ink spreading

In the printing process, inks are partially superposed in order to produce new colours. Under certain circumstances, the overlap of the printed inks causes further spreading of the dyes. This induces a significant dot gain and colour deviation. Note that the total amount of dyes remains constant throughout the spreading process, and only the spatial distribution is changed. The complex interaction between the inks and the printed surface is strongly related to physical properties like wettability and solvent absorption. As a consequence the inks behave differently on every surface. According to our experience, the local amount of solvent and the state of the surface ("wet" or "dry") are the main parameters to take into account. Printer and paper manufacturers try to minimize the unwanted ink spreading by developing special paper coatings.²³ Nevertheless, ink spreading still induces significant colour deviations which must be taken into account.

The ink spreading phenomenon can be modelled by modifying the size of the impact according to the configuration of its neighbouring drop impacts and the state of the surface. Since the amount of dyes remains constant, the maximal density D at the centre of the impact must decrease when the area a of the impact increases:

$$D = D_0 \cdot \left(\frac{a_0}{a}\right) \quad (19)$$

where a_0 and D_0 are respectively the area and the maximal density at the centre of an isolated impact.

By experimenting on a particular sample, we found a set of empirical rules which are slightly different for each ink-paper combination. First, we analyse the spreading of a drop printed on a dry surface by estimating under the microscope the enlargement of the impact when it is in contact with an increasing number of neighbouring impacts. Second, we estimate the enlargement caused by an ink drop printed on a "wet" surface, i.e., where another drop was already printed, as a function of the number of neighbouring impacts. We observed that the higher the number of neighbours covered with ink, the stronger the spreading. A neighbouring impact composed of the superposition of two ink drops increases the local amount of solvent. This also influences ink spreading but to a lower extent. Those results were summarized as a set of ink spreading rules which give the enlargement according to the configuration of the ink drop impacts (see Table 2).

As shown in the previous section, high resolution grids (one for each ink) are used to simulate the behaviour of the inks printed on the substrate. Each simulated impact is stamped on a high resolution grid and its size is modified according to our empirical ink spreading rules.

Prediction results

In a first step this model was applied to monochromatic patches. We predicted the spectra of 25 cyan halftoned samples generated with Bayer’s³ dithering method and printed using an HP DJ560 ink-jet printer. Note that this device prints coloured drops according to a hexagonal grid and the shape of the drop impact is circular. All 25 samples were printed on J21 paper from MPA²⁰ whose ink absorbing layer has a refractive index of $n = 1.5$. The ink spreading rules for this ink-paper combination are given in Table 2 in the column labelled “HP”. The samples were illuminated with a tungsten light source and their spectra were measured using an integrating sphere combined with a radiometer INSTASPEC II from Oriel.²² The samples were measured 24 hours after being printed. The same instrument was used to measure the reflectance of the paper in order to derive R_g . The absorption spectra of the cyan ink was measured on transparency with the same ink absorbing layer using the same radiometer with collimated light.

For good prediction accuracy, five inking levels are taken into account. This implies the use of larger matrices in equation (13). Furthermore, the grid point corresponds to a square surface element of $5 \times 5 \mu m$. In accordance with Oitinen’s study,²¹ the extent of our discrete PSF has a radius of about $100 \mu m$. As a consequence, the value of d in equation (18) is about $20 \mu m$. Note that at 300 dpi, the distance between two dot centres is $85 \mu m$. The integration of the PSF over the area of a neighbouring grid point gives the weight of this point.

Using our model and mathematical framework, we computed the spectra of the 25 halftoned cyan samples with an average prediction error of $\Delta E = 1.4$ and a maximal error of $\Delta E = 2.7$ in CIELAB. An example of a predicted spectrum is given in Figure 6, and the results are summarised in Table 1.

Table 1: Average prediction error in CIELAB, root mean square error and maximal deviation of predicted spectra of the series of cyan samples printed with an HP DJ 560C printer.

Series	Average ΔE	$\sqrt{\frac{\sum \Delta E^2}{n}}$	Maximal ΔE
25 cyan samples	1.40	1.51	2.67

In a second step the model predicted the spectra of samples printed with two inks, cyan and yellow. We produced four series of 25 samples i.e. a total of 100 samples. They correspond to the four combinations obtained by using two different halftoning methods with two different printers (having different inks and papers). The halftone methods used were a clustered dither algorithm with 33 levels of grey and Bayer’s³ dithering method. Two series were printed with an HP DJ560 ink-jet printer on J21 paper from MPA.²⁰ Two other series

were printed with an EPSON Stylus Color 900 ink-jet printer on “EPSON glossy photo quality” paper.⁹ All samples were measured with the same equipment used in the monochrome case.

The EPSON Stylus Color 900 printer was used in its 360 dpi mode. It also uses a hexagonal grid for coloured inks, but its drop impact is elliptic.

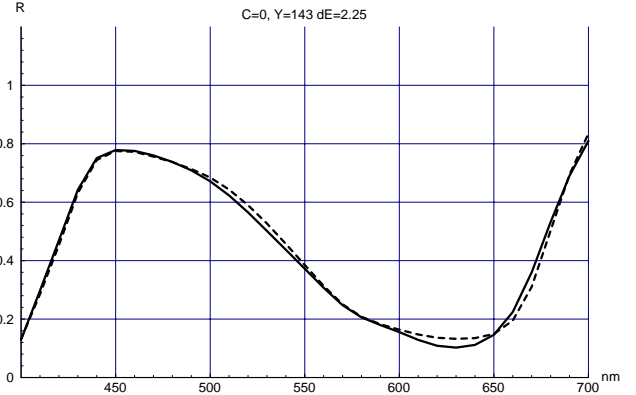


Figure 6. Measured spectrum (continuous line) and predicted spectrum (dashed line) of a halftoned cyan sample at level 143 printed with an HP DJ560C. The prediction error is $\Delta E = 2.25$ in CIELAB. (Note that level 0 means 100% ink coverage and level 255 means 0% ink coverage).

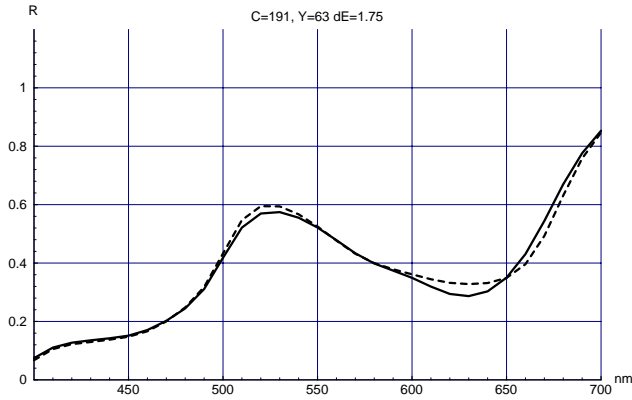
Table 2: Impact enlargement rules according to the state of the surface and the configuration of the dot neighbours. The enlargement is given in terms of area percentage. The “*” indicates that the rule in question does not apply.

Surface	Number of neighbours	Number of two-drop neighbours	HP	EPSON
Dry	>1	any	10%	10%
Wet	0	0	0%	32%
Wet	1	0	10%	32%
Wet	1	1	32%	32%
Wet	2	0	32%	32%
Wet	[3...5]	>1	56%	*
Wet	[3...4]	>0	*	44%
Wet	5	>1	*	96%
Wet	6	0	96%	44%
Wet	6	2	140%	140%
Wet	6	[3...5]	189%	189%
Wet	6	6	82%	82%

We simulated these samples on the high resolution grids using the previously described ink spreading model and light scattering model. As in the case of the monochromatic samples, the computer counted the grid points and their neighbours in order to find the relative area a_u occupied by each ink combination u and the scattering coefficients $\delta_{u,v}$ (see in the section “Simplified light scattering model”). Since five inking levels per ink are considered, a total of twenty five combinations must be taken into account. The computation of the reflection spectrum is the same as in the monochromatic case except that larger matrices are used in equation (13).

The average prediction error between measured and predicted spectra is about $\Delta E = 2.1$ and the maximal error is $\Delta E = 5$ in CIELAB. Two examples are given in Figure 7, and the results are listed in Tables 3, 4, 5 and 6. A summary is given in Table 7. Note that when ink spreading is not taken into account, the average prediction error is about $\Delta E = 10$.

a) Printed on an HP DJ560 C printer



b) Printed on an EPSON Stylus Color 900 printer

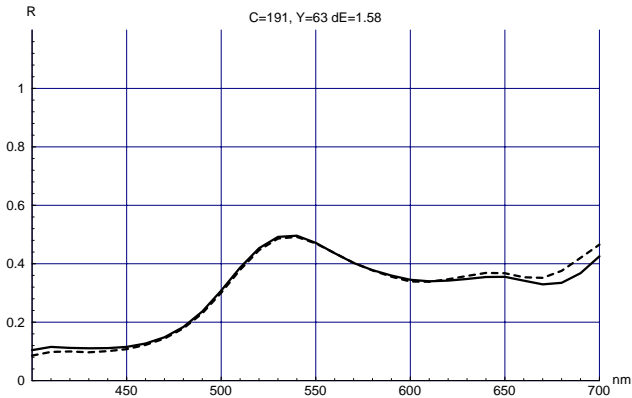


Figure 7. Measured spectra (continuous lines) and predicted spectra (dashed lines) of one half-toned green sample (clustered dither) printed on two different printers. The patche is a superposition of a cyan half-toned layer (level 191) and a yellow half-toned layer (level 127). Note that level 0 means 100% ink coverage and level 255 means 0% ink coverage.

Table 3: Bayer dither, printed with the HP printer. Measured colour, predicted colour and colour difference in CIELAB.

Levels	C=255			C=191			C=127			C=63			C=0		
	a	b	L	a	b	L	a	b	L	a	b	L	a	b	L
Y=255	1.	-3.	91.	-22.	-32.	72.	-41.	-50.	58.	-47.	-60.	50.	-47.	-65.	46.
	1.	-3.	92.	-24.	-30.	72.	-39.	-48.	59.	-45.	-58.	51.	-47.	-66.	45.
	0.3			1.9			2.7			2.3			0.4		
Y=191	1.	27.	90.	-24.	-4.	70.	-46.	-23.	56.	-54.	-30.	49.	-55.	-34.	44.
	1.	25.	91.	-25.	-4.	71.	-45.	-21.	57.	-52.	-28.	50.	-55.	-32.	44.
	1.5			1.6			2.4			2.2			1.9		
Y=127	2.	49.	90.	-29.	14.	67.	-51.	-5.	54.	-57.	-12.	47.	-53.	-16.	44.
	2.	47.	90.	-32.	12.	67.	-48.	-4.	55.	-51.	-12.	48.	-57.	-17.	44.
	1.8			3.7			3.3			1.9			4.7		
Y=63	4.	64.	90.	-35.	25.	65.	-55.	7.	52.	-56.	-1.	47.	-54.	-6.	43.
	3.	62.	90.	-36.	23.	65.	-53.	6.	53.	-56.	-2.	47.	-56.	-8.	43.
	2.3			2.7			2.5			1.5			3.2		
Y=0	5.	75.	89.	-41.	31.	61.	-54.	15.	51.	-57.	7.	45.	-55.	1.	42.
	4.	75.	90.	-43.	30.	62.	-58.	12.	52.	-58.	4.	46.	-55.	2.	42.
	0.9			2.1			5.1			2.9			0.6		

Table 4: Clustered dither, printed with the HP printer. Measured colour, predicted colour and colour difference in CIELAB.

Levels	C=255			C=191			C=127			C=63			C=0		
	a	b	L	a	b	L	a	b	L	a	b	L	a	b	L
Y=255	1.	-3.	91.	-15.	-24.	76.	-26.	-39.	65.	-38.	-54.	54.	-47.	-65.	46.
	1.	-3.	92.	-15.	-24.	76.	-26.	-40.	65.	-41.	-55.	53.	-47.	-66.	45.
	0.2			0.9			0.8			3.			1.3		
Y=191	1.	19.	91.	-16.	-5.	75.	-28.	-20.	64.	-42.	-34.	53.	-53.	-43.	44.
	1.	20.	91.	-17.	-4.	75.	-29.	-18.	64.	-44.	-33.	52.	-53.	-42.	44.
	1.2			2.3			2.8			2.2			1.7		
Y=127	2.	38.	90.	-17.	12.	74.	-29.	-4.	63.	-46.	-19.	51.	-56.	-26.	43.
	2.	40.	90.	-20.	12.	73.	-32.	-3.	62.	-46.	-17.	51.	-55.	-24.	44.
	1.4			2.4			2.8			1.1			1.7		
Y=63	4.	59.	89.	-20.	30.	71.	-33.	14.	60.	-49.	-1.	50.	-56.	-9.	43.
	3.	59.	90.	-19.	31.	72.	-33.	13.	60.	-49.	-2.	49.	-56.	-9.	43.
	0.9			1.8			1.2			1.			0.4		
Y=0	5.	75.	89.	-24.	43.	69.	-40.	24.	56.	-54.	9.	47.	-54.	1.	42.
	4.	75.	90.	-22.	43.	70.	-39.	23.	58.	-55.	8.	47.	-55.	2.	42.
	0.9			2.6			2.1			1.7			1.		

Table 5: Bayer dither, printed with the EPSON printer. Measured colour, predicted colour and colour difference in CIELAB.

Levels	C=255			C=191			C=127			C=63			C=0		
	a	b	L	a	b	L	a	b	L	a	b	L	a	b	L
Y=255	1.	-2.	94.	-19.	-33.	72.	-33.	-54.	57.	-37.	-65.	48.	-41.	-73.	41.
	1.	-2.	94.	-18.	-32.	73.	-35.	-54.	57.	-39.	-63.	50.	-43.	-70.	43.
	0.1			2.1			2.			3.2			3.8		
Y=191	3.	35.	92.	-23.	5.	68.	-37.	-15.	54.	-44.	-24.	45.	-49.	-32.	38.
	3.	35.	92.	-22.	2.	68.	-38.	-18.	53.	-43.	-27.	47.	-48.	-35.	40.
	0.8			3.1			3.3			4.			4.		
Y=127	5.	62.	91.	-20.	28.	67.	-39.	6.	51.	-44.	-3.	43.	-47.	-10.	37.
	7.	64.	90.	-19.	27.	66.	-39.	5.	50.	-45.	-4.	44.	-48.	-10.	39.
	2.6			1.5			1.7			1.9			2.4		
Y=63	8.	76.	90.	-19.	39.	65.	-38.	17.	50.	-43.	6.	42.	-45.	-1.	37.
	9.	76.	90.	-18.	37.	64.	-39.	15.	50.	-44.	6.	42.	-45.	1.	36.
	1.			2.2			2.6			0.5			2.2		
Y=0	10.	87.	89.	-17.	48.	64.	-38.	23.	48.	-42.	11.	40.	-42.	5.	36.
	11.	88.	89.	-16.	48.	63.	-38.	23.	48.	-42.	12.	39.	-45.	7.	36.
	1.3			1.2			0.8			1.7			3.2		

Table 6: Clustered dither, printed with the EPSON printer. Measured colour, predicted colour and colour difference in CIELAB.

Levels	C=255 a b L	C=191 a b L	C=127 a b L	C=63 a b L	C=0 a b L
Y=255	1. -2. 94. 1. -2. 94. 0.2	-12. -26. 76. -12. -25. 77. 2.3	-19. -42. 64. -21. -41. 65. 2.4	-30. -58. 52. -33. -58. 53. 3.4	-42. -73. 41. -43. -70. 43. 3.9
Y=191	3. 26. 92. 3. 26. 92. 0.3	-14. -0. 73. -14. 1. 74. 1.6	-20. -14. 62. -22. -13. 63. 2.3	-31. -30. 50. -35. -29. 50. 4.1	-45. -44. 39. -46. -43. 41. 2.7
Y=127	6. 46. 91. 6. 48. 91. 1.4	-14. 16. 71. -13. 17. 71. 1.7	-21. 2. 59. -23. 3. 60. 2.2	-30. -12. 49. -34. -10. 49. 4.5	-45. -26. 38. -47. -22. 39. 4.9
Y=63	8. 68. 90. 9. 70. 90. 1.4	-12. 36. 69. -11. 38. 69. 1.6	-22. 18. 57. -24. 19. 57. 1.6	-32. 4. 47. -35. 5. 46. 4.	-44. -7. 37. -46. -5. 37. 3.6
Y=0	10. 87. 89. 11. 88. 89. 1.5	-10. 54. 67. -7. 57. 69. 4.6	-21. 35. 55. -22. 34. 54. 1.8	-34. 17. 44. -36. 17. 43. 2.7	-43. 4. 36. -45. 7. 36. 3.2

Table 7: Average prediction error in CIELAB, root mean square error and maximal deviation for each cyan-yellow series of predicted spectra.

Series	Average ΔE	$\sqrt{\frac{\sum \Delta E^2}{n}}$	Maximal ΔE
Bayer dither on HP printer	2.25	2.53	5.08
Clustered dither on HP printer	1.57	1.75	2.95
Bayer dither on EPSON printer	2.10	2.34	3.96
Clustered dither on EPSON printer	2.56	2.85	4.92

Conclusions

We introduced a new mathematical framework based on matrices. This global approach incorporates all significant physical contributing phenomena. We introduced light scattering coefficients which could also be changed to suit other models of light scattering in paper. We have shown that classical results such as the Murray-Davis and the Clapper-Yule formulas correspond to particular cases of our model.

We modelled the spreading process by enlarging the drop impact according to the configuration of its neighbours and the state of the surface. The printed surface was simulated using high resolution grids. This allowed us to compute the relative areas occupied by the various ink-combinations and the corresponding light scattering coefficients $\delta_{u,v}$.

The spectra of halftoned samples produced with one ink were predicted with an average prediction error of about $\Delta E = 1.4$ in CIELAB. For two halftoned ink layers, we also achieved good spectral predictions with an average error of

about $\Delta E = 2.1$ in CIELAB.

Currently we are extending the experimental set to other ink combinations and other ink-jet printers. The complexity of ink spreading requires deeper investigation in order to predict the behaviour of three ink combinations.

Acknowledgment

We would like to thank Dr. P. Heinzer from MPA for providing useful information on ink-jet paper, and the Swiss National Science Foundation (grant No. 21-54127.98) for supporting the project.

References

1. J.S. Arney, "Probability Description of the Yule-Nielsen Effect, I," *Journal of Imaging Science and Technology*, Vol. **41**, No. 6, November/December 1997, pp. 633-636.
2. J.S. Arney, T. Wu, C. Blehm, "Modeling the Yule-Nielsen Effect on Color Halftones," *Journal of Imaging Science and Technology*, Vol. **42**, No 4, July/August 1998, pp. 335-340.
3. B.E. Bayer, "An Optimum Method for Two-Level Rendition of Continuous-Tone Pictures," *IEEE 1973 International Conference on Communications*, Vol. **1**, June 1973, pp. 26-11—26-15.
4. W.E. Boyce, R.C. DiPrima, *Elementary Differential Equations and Boundary Value Problems*, Sixth Edition, John Wiley & Sons, New York, 1997, pp. 401-405.
5. F.R. Clapper, J.A.C. Yule, "The Effect of Multiple Internal Reflections on the Densities of Half-tone Prints on Paper," *Journal of the Optical Society of America*, Vol. **43**, No. 7, July 1953, pp. 600-603.
6. P. Emmel, *Modèles de Prédiction Couleur Appliqués à l'Impression Jet d'Encre*, PhD thesis No. 1857, Ecole Polytechnique Fédérale de Lausanne (EPFL), Lausanne, Switzerland, 1998, pp. 55-58, <http://diwww.epfl.ch/w3lsp/publications/colour/thesis-emmel.html> (in French).
7. P. Emmel, *Modèles de Prédiction Couleur Appliqués à l'Impression Jet d'Encre*, PhD thesis No. 1857, Ecole Polytechnique Fédérale de Lausanne (EPFL), Lausanne, Switzerland, 1998, p. 114, <http://diwww.epfl.ch/w3lsp/publications/colour/thesis-emmel.html> (in French).
8. P. Emmel, R. D. Hersch, "Towards a Color Prediction Model for Printed Patches," *IEEE Computer Graphics and Applications*, Vol. **19**, No. 4, July/August 1999, pp. 54-60.
9. <http://www.epson.com>
10. S. Gustavson, *Dot Gain in Colour Halftones*, PhD thesis No. 492, Linköping University, Linköping, Sweden, September 1997.
11. S. Gustavson, *Dot Gain in Colour Halftones*, PhD thesis No. 492, Linköping University, Linköping, Sweden, September 1997, p. 55.
12. D.B. Judd, "Fresnel Reflection of Diffusely Incident Light," *Journal of the National Bureau of Standards*, Vol. **29**, November 1942, pp. 329-332.
13. D.B. Judd, G. Wyszecki, *Color in Business, Science and*

- Industry*, Third Edition, John Wiley & Sons, 1975, pp. 415-417.
14. D.B. Judd, G. Wyszecki, *Color in Business, Science and Industry*, Third Edition, John Wiley & Sons, 1975, pp. 426-431.
 15. H.R. Kang, *Color Technology for Electronic Imaging Devices*, SPIE Optical Engineering Press, Bellingham WA, USA, 1997, pp. 42-43.
 16. P. Kubelka, F. Munk, "Ein Beitrag zur Optik der Farbanstriche," *Zeitschrift für technische Physik*, Vol. **12**, 1931, pp. 593-601.
 17. R. McDonald Editor, *Colour Physics for Industry*, Second Edition, The Society of Dyers and Colourists, Bradford, UK, 1997, p. 299.
 18. R. McDonald Editor, *Colour Physics for Industry*, Second Edition, The Society of Dyers and Colourists, Bradford, UK, 1997, pp. 304-307.
 19. R. McDonald Editor, *Colour Physics for Industry*, Second Edition, The Society of Dyers and Colourists, Bradford, UK, 1997, p. 306.
 20. <http://www.mpa.ch>
 21. P. Oittinen, H. Saarelma, "Influence of optical surface properties of paper on information capacity," *Paperi ja puu - Paper and Timber*, Vol. **75**, No. 1-2, 1993, pp. 66-71.
 22. <http://www.LOT-Oriel.com>
 23. A. Owatari et al., *Ink Jet Recording Medium*, United States Patent No. 5,928,787, July 1999.
 24. G.L. Rogers, "Optical dot gain in halftone print," *Journal of Imaging Science and Technology*, Vol. **41**, No. 6, 1997, pp. 643-656.
 25. G.L. Rogers, "Effect of Light Scatter on Halftone Color," *Journal of the Optical Society of America A*, Vol. **15**, No. 7, July 1998, pp. 1813-1821.
 26. F.R. Ruckdeschel, O.G. Hauser, "Yule-Nielsen effect in printing: a physical analysis," *Applied Optics*, Vol. **17**, No. 21, November 1978, pp. 3376-3383.
 27. J.L. Saunderson, "Calculation of the Color Pigmented Plastics," *Journal of the Optical Society of America*, Vol. **32**, December 1942, pp. 727-736.
 28. G. Wyszecki, W.S. Stiles, *Color Science: Concepts and Methods, Quantitative Data and Formulae*, Second Edition, John Wiley & Sons, 1982, pp. 235-240.